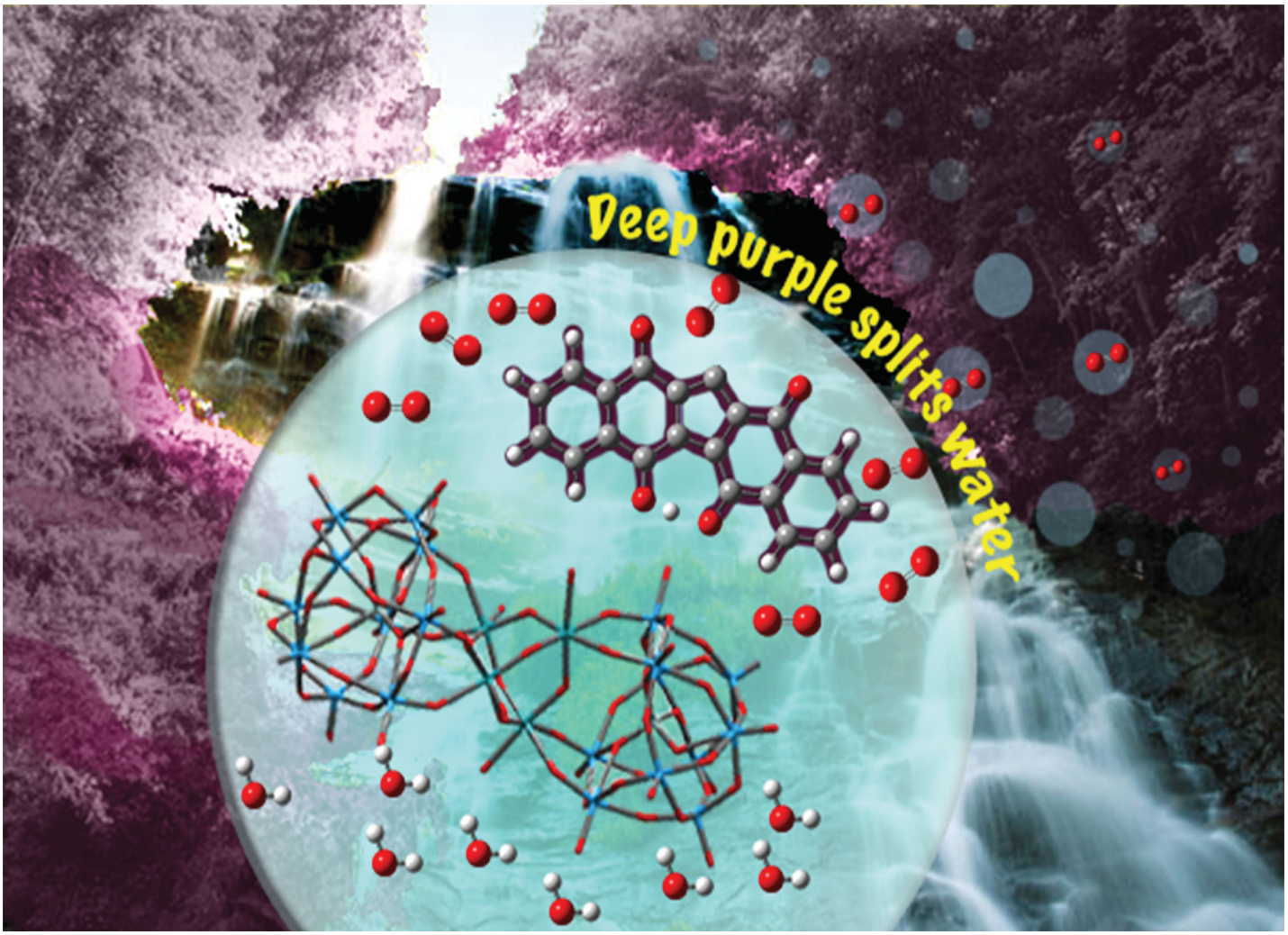

Showcasing research from a joint collaboration between the groups of Prof. Pierluca Galloni at the Department of Chemical Science and Technologies, University of Rome "Tor Vergata" and of Prof. Andrea Sartorel at the Department of Chemical Sciences, University of Padova, Italy.

Photoanodes for water oxidation with visible light based on a pentacyclic quinoid organic dye enabling proton-coupled electron transfer

This works presents a novel pool of chromophores for photoelectrochemical applications aimed at solar light conversion, within artificial photosynthetic schemes.

As featured in:

See Serena Berardi, Pierluca Galloni, Andrea Sartorel *et al.*, *Chem. Commun.*, 2020, **56**, 2248.

ROYAL SOCIETY OF CHEMISTRY

rsc.li/chemcomm

Registered charity number: 207890

ChemComm

COMMUNICATION

View Article Online
View Journal | View Issue

Cite this: *Chem. Commun.*, 2020, **56**, 2248

Received 18th December 2019,
Accepted 21st January 2020

DOI: 10.1039/c9cc09805d

rsc.li/chemcomm

Photoanodes for water oxidation with visible light based on a pentacyclic quinoid organic dye enabling proton-coupled electron transfer†

Giulia Alice Volpato, ‡[a] Martina Marasi, ‡[ab] Thomas Gobbato, [a] Francesca Valentini, [b] Federica Sabuzi, [b] Valeria Gagliardi, [ab] Alessandro Bonetto, [c] Antonio Marcomini, [c] Serena Berardi, *[d] Valeria Conte, [b] Marcella Bonchio, [a] Stefano Caramori, [d] Pierluca Galloni *[b] and Andrea Sartorel *[a]

A pentacyclic quinoid dye, $KuQ(O)_3OH$, combining (i) extended visible absorption up to 600 nm, (ii) excited state reduction potential >2 V *vs.* NHE, and (iii) a photoinduced proton-coupled electron transfer mechanism, has been used for the fabrication of dye-sensitized SnO_2 photoanodes integrating a ruthenium polyoxometalate water oxidation catalyst. The resulting photoelectrode $SnO_2|KuQ(O)_3OH|$-Ru_4POM displays a light harvesting efficiency up to 90% in the range 500–600 nm, an onset potential as low as 0.2 V *vs.* NHE at pH 5.8, photoinduced oxygen evolution with a faradaic efficiency of 70 ± 15% and an absorbed-photon-to-current efficiency up to 0.12 ± 0.01%.

Photoelectrochemical cells (PECs) are a promising technology for converting solar energy into chemical fuels, *i.e.* by means of light-induced water splitting.[1] The development of dye-sensitized photoelectrodes for PECs is one of the current strategies to exploit solar radiation in the visible region.[2] Photoanodes for water oxidation have been developed with dyes comprising ruthenium(II) polypyridine derivatives,[3] porphyrinoids,[4] BODIPY,[5] perylenes,[6] polymeric films,[7] and triarylamines.[8] In particular, the use of molecularly defined organic chromophores provides the advantages of tuning the spectroscopic and redox properties, while avoiding the use of rare transition metals.[2,4–8]

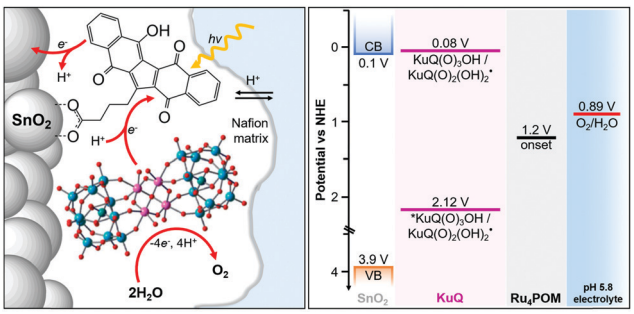

Scheme 1 Schematic representation of the $SnO_2|KuQ(O)_3OH|Ru_4POM$ photoanode for water oxidation. The energy levels are shown for the system at pH = 5.8.

In this work, we exploit a pentacyclic quinoid organic dye[9] 1-(3-carboxypropyl)KuQuinone ($KuQ(O)_3OH$) anchored onto a nanostructured tin oxide semiconductor to achieve photoelectrochemical water oxidation, when integrated with a ruthenium polyoxometalate catalyst (Ru_4POM),[6d,10a] Scheme 1.

Besides being a novel class of dyes for this application, two significant features distinguish $KuQ(O)_3OH$ from the pool already developed in the literature: (i) the ability to manage proton-coupled electron transfer (PCET), which is a peculiar feature of water oxidation photosynthetic schemes[11] and (ii) a "non-classical" mechanism, based on the reductive quenching of the excited state of the dye, followed by electron injection into the semiconductor conduction band.

KuQuinone dyes show extended absorption in the visible region.[9] In tetrahydrofuran solution, $KuQ(O)_3OH$ presents two intense absorption maxima (λ_1 = 563 nm, $\varepsilon^{563} = 1.5 \times 10^4$ M^{-1} cm^{-1}; λ_2 = 529 nm, $\varepsilon^{529} = 1.17 \times 10^4$ M^{-1} cm^{-1}), redshifted with respect to those observed for the deprotonated enolate $KuQ(O)_3O^-$ (λ_1 = 534 nm, $\varepsilon^{534} = 7.2 \times 10^3$ M^{-1} cm^{-1}; λ_2 = 504 nm $\varepsilon^{504} = 8.4 \times 10^3$ M^{-1} cm^{-1}), Fig. S1 in the ESI.† Time-dependent density functional calculations at the B3LYP/6-31g+(d,p) level of theory, including a polarizable continuum model of the solvent, assign the lowest energy absorption bands to the

[a] *Department of Chemical Sciences, University of Padova, Via Marzolo 1, 35131 Padova, Italy. E-mail: andrea.sartorel@unipd.it*
[b] *Department of Chemical Science and Technologies, University of Rome "Tor Vergata", via della Ricerca Scientifica, snc 00133 Roma, Italy. E-mail: galloni@scienze.uniroma2.it*
[c] *Department of Environmental Sciences, Informatics and Statistics, University Ca' Foscari Venice, Vegapark, Via delle Industrie 21/8, 30175 Marghera, Venice, Italy*
[d] *Department of Chemical and Pharmaceutical Sciences, University of Ferrara, and Centro Interuniversitario per la Conversione Chimica dell'Energia Solare (SolarChem), sez. di Ferrara, Via L. Borsari 46, 44121 Ferrara, Italy. E-mail: brrsrn@unife.it*

† Electronic supplementary information (ESI) available: Full experimental procedures, and additional characterization of the dye and of the photoelectrodes. See DOI: 10.1039/c9cc09805d

‡ These authors contributed equally.

HOMO → LUMO transitions, with both orbitals delocalized on the extended aromatic scaffold (Fig. S2 in ESI†).[9] The emission properties of the dye are influenced by the acid–base equilibria occurring at the ground and excited states. Emission spectra show broad bands with maxima in the range 560–600 nm (quantum yields 1.1–7.9%), decaying with lifetimes of 0.63–3.57 ns, consistent with singlet excited states (Fig. S3 and S4 in ESI†). From the intersection of the normalized absorption and emission, it is possible to estimate an $E^{0\text{-}0}$ energy of 2.16 eV and 2.28 eV for $KuQ(O)_3OH$ and $KuQ(O)_3O^-$, respectively, and $E^{0\text{-}0} \approx 2.04$ eV when the dye is anchored onto SnO_2 under the operative conditions employed in this work (pH 5.8), *vide infra*.

Notably, the reduction potential of $KuQ(O)_3OH$ drop-cast onto a glassy carbon electrode falls in the range 0.116–0.078 V *vs.* NHE in aqueous electrolyte (0.1 M $Na_2SiF_6/NaHCO_3$ buffer, pH in the range 5.2–5.9),§ and depends on pH with a slope of 58 ± 1 mV per unit, indicative of a PCET involving a $KuQ(O)_3OH/KuQ(O)_2(OH)_2^{\bullet}$ couple (Fig. 1a and Fig. S6 in ESI†).¶ Merging the electrochemical properties and the $E^{0\text{-}0}$ energy of 2.04 eV previously determined, the reduction potential of the excited state ($^*KuQ(O)_3OH/KuQ(O)_2(OH)_2^{\bullet}$ couple) stands in the range +2.12 to +2.16 V *vs.* NHE.[12] Thus, the $^*KuQ(O)_3OH$ excited state is a very powerful oxidant, to be considered for application in the photoelectrochemical oxidation of water (E = 0.89 V *vs.* NHE at pH 5.8 for O_2/H_2O couple, Scheme 1, right). In addition, the LUMO energy level is suitable for coupling the $KuQ(O)_3OH$ dye with semiconductors such as SnO_2 (conduction band at + 0.1 V *vs.* NHE, Scheme 1, right).[13]

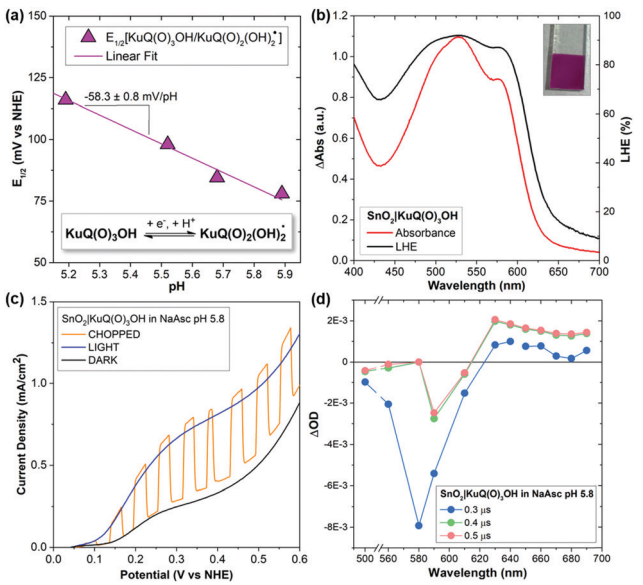

Fig. 1 (a) Plot of $E_{1/2}$ *vs.* pH for the $KuQ(O)_3OH/KuQ(O)_2(OH)_2^{\bullet}$ couple. Inset: Scheme of proton-coupled electron transfer associated with the dye. (b) Absorption spectrum and light harvesting efficiency (LHE) of the $SnO_2|KuQ(O)_3OH$ photoanode, after subtraction of the SnO_2 contribution. Inset: Photograph of the $SnO_2|KuQ(O)_3OH$ photoanode. (c) LSV registered for $SnO_2|KuQ(O)_3OH$ in 0.1 M sodium ascorbate at pH = 5.8 under dark and light conditions and under chopped irradiation (CE: Pt; RE: Ag/AgCl 3 M NaCl; 20 mV s^{-1}; iR drop compensated, see Section 2.5 in ESI;† light: AM 1.5G + 400 nm cut-off filter). (d) Transient absorption spectra of a $SnO_2|KuQ(O)_3OH$ at different time delays after the 532 nm ns-laser excitation pulse, recorded in 1 M sodium ascorbate at pH = 5.8.

Grafting of $KuQ(O)_3OH$ onto nanostructured SnO_2 was achieved by soaking the electrode overnight into a 0.13 mM solution of $KuQ(O)_3OH$ in tetrahydrofuran. The carboxylate function in the lateral chain allows a notable surface loading of 140 ± 20 nmol cm^{-2} to be reached (see ESI†).‖ The absorbance spectrum of the $SnO_2|KuQ(O)_3OH$ photoanode shows the fingerprint of the dye, with a light harvesting efficiency (LHE) of *ca.* 90% in the range 500–600 nm (Fig. 1b). The photoelectrochemical properties of $SnO_2|KuQ(O)_3OH$ were tested by linear sweep voltammetry (LSV) in aqueous 0.1 M ascorbate electron donor at pH = 5.8 (*i.e.*, the same pH used in photoelectrochemical water oxidation, *vide infra*), in order to verify the ability of the dye to inject electrons into the semiconductor, evaluating the onset potential and photocurrent density, together with the electron injection mechanism.** Comparing the LSV scans under dark and irradiation conditions, the raising of the photocurrent is observed at an onset potential of 0.1 V *vs.* NHE, reaching a photocurrent plateau of 0.4 mA cm^{-2} at *ca.* 0.4 V (Fig. 1c; at $E > 0.2$ V a dark current due to oxidation of ascorbate is also observed). Transient absorption spectroscopy (TAS) experiments evidence the formation of the $KuQ(O)_2(OH)_2^{\bullet}$, a reduced form of the dye, associated with the long-living absorption at $\lambda > 610$ nm (>1.5 μs Fig. 1d; this assignment is corroborated by the comparison with the TAS spectrum obtained for the $KuQ(O)_3OH$ dye in THF solution containing ascorbate, Fig. S8 in ESI†). Therefore, the mechanism under these conditions is based on the dye excitation and subsequent reductive quenching of the $^*KuQ(O)_3OH$ excited state by the ascorbate donor to form the reduced $KuQ(O)_2(OH)_2^{\bullet}$, which is then responsible for electron injection into the conduction band of SnO_2 (Scheme 1).

These results prompted us to combine the $SnO_2|KuQ(O)_3OH$ electrode with a tetraruthenium polyoxometalate water oxidation catalyst $Na_{10}\{Ru_4(\mu\text{-}O)_4(\mu\text{-}OH)_2[\gamma\text{-}SiW_{10}O_{36}]_2\}$, hereafter Ru_4POM (see CV in Fig. S9, ESI†),[10] that was already exploited in photoelectrodes with Ru polypyridine[10b,c] and perylene bisimide chromophores.[6d] Functionalization of the $SnO_2|KuQ(O)_3OH$ electrode with Ru_4POM was achieved by 30 minutes soaking into a 4 mM aqueous solution of Ru_4POM containing 1% m/v Nafion polymer,[14] followed by rinsing in water (13 ± 5 nmol cm^{-2} loading of Ru_4POM as revealed by inductively coupled plasma mass spectrometry, ICP-MS).††

Absorption spectrum of the $SnO_2|KuQ(O)_3OH|Ru_4POM$ photoanode (Fig. S10 in ESI†) shows an overall enhanced absorption in the visible region, consistent with the absorption features of Ru_4POM. Atomic force microscopy (AFM) and scanning electron microscopy (SEM) images (Fig. 2a and Fig. S11, S12, ESI†) reveal a smoothing of the surface with respect to the $SnO_2|KuQ(O)_3OH$ electrode, ascribable to the presence of the Nafion polymer. EDX elemental mapping (Fig. S13 and S14, ESI†) evidences the homogenous distribution of Ru_4POM and Nafion over the surface and, more importantly, through the whole 3 μm-thick layer of mesoporous SnO_2.

LSV experiments under dark and light conditions with the $SnO_2|KuQ(O)_3OH|Ru_4POM$ electrode are reported in Fig. 2b.‡‡

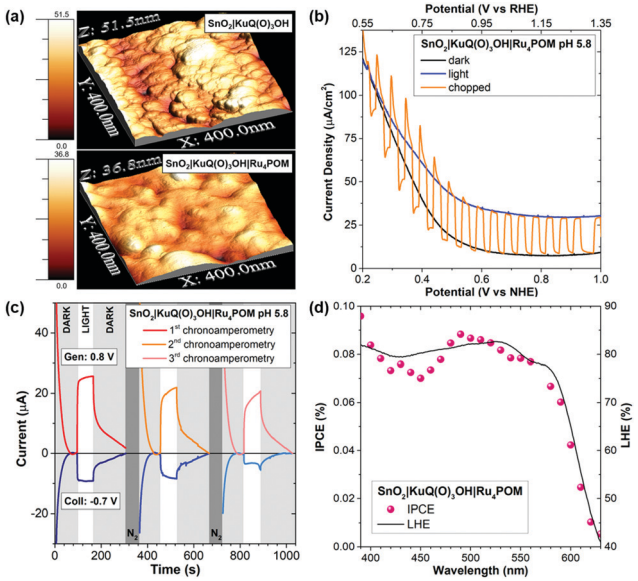

Fig. 2 (a) AFM images of $SnO_2|KuQ(O)_3OH$ and $SnO_2|KuQ(O)_3OH|Ru_4POM$ photoanodes. (b) LSV for $SnO_2|KuQ(O)_3OH|Ru_4POM$ in 0.1 M Na_2SiF_6/$NaHCO_3$ buffer pH 5.8 (CE: Pt; RE: Ag/AgCl 3 M NaCl; 20 mV s^{-1}; light: AM 1.5G + 400 nm cut-off filter). (c) Consecutive G–C experiments for O_2 detection with $SnO_2|KuQ(O)_3OH|Ru_4POM$ in 0.1 M Na_2SiF_6/$NaHCO_3$ buffer pH 5.8; the positive photocurrent (red, orange, and pink traces) is accompanied by a negative current of O_2 reduction at the FTO collector (blue, light blue, and azure traces); CE: Pt; RE: Ag/AgCl 3 M NaCl; light: white LED + 400 nm cut-off filter, see ESI.† (d) IPCE (purple dots) obtained in Na_2SiF_6/$NaHCO_3$ buffer pH 5.8 and light harvesting efficiency (black line) of $SnO_2|KuQ(O)_3OH|Ru_4POM$.

The dark scan (black trace) shows an initial dark current density, stabilizing at *ca.* 10 μA cm^{-2} at potentials >0.6 V *vs.* NHE (corresponding to 0.95 V *vs.* reversible hydrogen electrode, RHE). This dark current contribution, occurring at potentials far below the one of the dark water oxidation process (E = 1.23 V *vs.* RHE) and not associated with oxygen evolution, is originated by the re-oxidation of Sn(III) generated when the cell is switched on at potentials corresponding to the Sn(IV)/(III) process, and by redox processes of Ru_4POM (Fig. S9 in ESI†); a further capacitive contribution arises from the presence of the Nafion layer. Under irradiation (blue trace and chopped orange trace), a photocurrent is observed starting at a low onset potential of 0.20 V *vs.* NHE (0.55 V *vs.* RHE), while reaching a net and constant value of 20 μA cm^2 in the range 0.4–1 V *vs.* NHE (0.75–1.35 V *vs.* RHE). The attribution of the observed photocurrent to oxygen evolution was confirmed through a generator–collector (G–C) method, where the anodic photocurrent produced at the $SnO_2|KuQ(O)_3OH|Ru_4POM$ generator held at 0.8 V *vs.* NHE (1.15 V *vs.* RHE) is accompanied by a cathodic current of oxygen reduction at an FTO collector, held at −0.7 V *vs.* NHE (Fig. 2c, see the Methods section and Fig. S15 and S16 in ESI†).[6d,15] A faradaic efficiency for photoinduced oxygen evolution of 70 ± 15% was thus estimated (see Table S2 in ESI†). Conversely, in the case of the catalyst-free $SnO_2|KuQ(O)_3OH$ electrode (stationary photocurrent of *ca.* 8 μA), no significant cathodic current for oxygen reduction is produced (Fig. S17, ESI†), confirming the fundamental role of Ru_4POM in driving water oxidation.

The incident photon-to-current efficiency (IPCE) reflects remarkably well the absorption spectrum of the photoanode, with a peak value of 0.09% at 490 nm (Fig. 2d). This value is similar to those obtained with KuQuinone derivatives deposited onto flat ITO substrates, in the presence of amines as sacrificial electron donors.[9d] The internal quantum efficiency (absorbed photon-to-current Efficiency, APCE = IPCE/LHE) is nearly constant in the 400–550 nm region of the spectrum, with an average value around 0.12 ± 0.01%. Benchmark metrics for dye-sensitized photoanodes for water oxidation are reported in Table S3 in the ESI;† in this scenario, the $SnO_2|KuQ(O)_3OH|Ru_4POM$ electrode is characterized by a low onset potential, while reaching the photocurrent density, faradaic efficiency and IPCE/APCE observed for electrodes sensitized with engineered Ru(II) polypyridine chromophores and the same Ru_4POM catalyst.

The charge transfer dynamics were preliminarily investigated by TAS. However, traces obtained for $SnO_2|KuQ(O)_3OH|Ru_4POM$ did not reveal diagnostic transient absorption features, and thus were poorly informative. The dye and catalyst were then assembled on insulating ZrO_2 films, characterised by a high energy conduction band that precludes electron injection, in order to favour the accumulation of stationary intermediates. For $ZrO_2|KuQ(O)_3OH$, laser irradiation led to the formation of a transient absorption, decaying in several μs (Fig. S18, ESI†), which is ascribable to the lowest triplet excited state of $KuQ(O)_3OH$, populated by intersystem crossing from the singlet excited state, in the absence of quenching species. Conversely, in $ZrO_2|KuQ(O)_3OH|Ru_4POM$, the absence of such long lived dynamics suggests a fast evolution of the dye excited state in the presence of Ru_4POM, and likely involving a charge transfer from Ru_4POM to $^*KuQ(O)_3OH$, forming oxidized Ru_4POM and reduced $KuQ(O)_2(OH)_2^{\bullet}$. However, no feature of this charge separated state are observed in the ns–μs domain, as the result of fast recombination that may thus limit the overall quantum efficiency under photoelectrochemical conditions.

Concerning stability, a decrease of photocurrent density was observed during 90 minutes of photoelectrolysis, with a drop to 60% of the initial value after 30 minutes, and to *ca.* 30% after 90 minutes (Fig. S19 in ESI†). This is associated with a visible leaching of $KuQ(O)_3OH$ dye and the Ru_4POM catalyst from the electrode: 1.75 ± 0.25 nmol cm^{-2} of Ru_4POM was quantified by ICP-MS on the stressed electrodes, accounting for 13% of the initial loading; a further engineering of the photoanode is thus required to improve long term stability, which is however a diffused issue in molecular-based photoanodes.[3–8]

In conclusion, we have reported a novel photoanode for water oxidation based on an organic quinoid dye, with a strong absorption in the visible region (up to 600 nm, $\varepsilon \approx 1.5 \times 10^4$ M^{-1} cm^{-1}), having a highly oxidizing excited state (E > 2 V *vs.* NHE) and that is capable of promoting photoinduced proton-coupled electron transfer. The $SnO_2|KuQ(O)_3OH|Ru_4POM$ performs photoelectrochemical water oxidation at a low onset potential, with a faradaic efficiency of 70 ± 15%, and IPCE and APCE values of 0.09% and 0.12 ± 0.01%, respectively. These results offer a new possibility for the design and realization of dye-sensitized devices for photocatalytic applications.

This work was supported by the Department of Chemical Sciences at the University of Padova (P-DISC "Phoetry" #10BIRD2018-UNIPD) and by Fondazione Cariparo ("Synergy", Progetti di Eccellenza 2018). V. G. thanks Regione Lazio for a scholarship (Project "TornoSubito"). We thank Sara Bonacchi for assistance in spectroscopic characterization of $KuQ(O)_3OH$.

Conflicts of interest

There are no conflicts to declare.

Notes and references

§ The $Na_2SiF_6/NaHCO_3$ buffer has been largely used in light driven water oxidation, and is the optimum choice for homogeneous systems employing Ru_4POM, see ref. 16.

¶ A second reversible wave is observed at *ca.* 0.2 V more negative potentials, and attributed to the deprotonated dye involving the $KuQ(O)_3O^-$/$KuQ(O)_3OH^{\bullet -}$ couple (Fig. S6 in ESI†).

‖ After the sensitization procedure, the photoanodes present an intense orange colour ascribed to the deprotonated $KuQ(O)_3O^-$, and likely originated from acid/base reaction with the SnO_2 surface. Dipping the electrodes in aqueous sulfuric acid (pH 2) leads to a colour change to deep violet, typical of $KuQ(O)_3OH$. This treatment significantly enhances the stability of $SnO_2|KuQ(O)_3OH$ in water up to several hours.

** Photocurrent densities of 20–30 μA cm^{-2} were observed with Br^- and triethanolamine donors in acidic and alkaline conditions, respectively, see Table S1 and Fig. S7 in ESI.†

†† In the absence of Nafion, a lower loading of 5 ± 1 nmol cm^{-2} Ru_4POM was obtained, with its immediate leaching when the electrodes were dipped in aqueous solution.

‡‡ Under these conditions, the electrode remains deep violet, indicative of the persistence of the $KuQ(O)_3OH$ form.

1 (*a*) K. Park, Y. J. Kim, T. Yoon, S. David and Y. M. Song, *RSC Adv.*, 2019, **9**, 30112–30124; (*b*) L. Steier and S. Holliday, *J. Mater. Chem. A*, 2018, **6**, 21809–21826; (*c*) J. R. McKone, N. S. Lewis and H. B. Gray, *Chem. Mater.*, 2014, **26**, 407–414.

2 (*a*) J. T. Kirner and R. G. Finke, *J. Mater. Chem. A*, 2017, **5**, 19560–19592; (*b*) P. Xu, N. S. McCool and T. E. Mallouk, *Nano Today*, 2017, **14**, 42–58; (*c*) Z. Yu, F. Li and L. Sun, *Energy Environ. Sci.*, 2015, **8**, 760–775.

3 (*a*) Y. Gao, X. Ding, J. Liu, L. Wang, Z. Lu, L. Li and L. Sun, *J. Am. Chem. Soc.*, 2013, **135**, 4219–4222; (*b*) J. W. Youngblood, S. H. A. Lee, Y. Kobayashi, E. A. Hernandez-Pagan, P. G. Hoertz, T. A. Moore, A. L. Moore, D. Gust and T. E. Mallouk, *J. Am. Chem. Soc.*, 2009, **131**, 926–927.

4 (*a*) A. O. Biroli, F. Tessore, G. Di Carlo, M. Pizzotti, E. Benazzi, F. Gentile, S. Berardi, C. A. Bignozzi, R. Argazzi, M. Natali, A. Sartorel and S. Caramori, *ACS Appl. Mater. Interfaces*, 2019, **11**, 32895–32908; (*b*) G. F. Moore, J. D. Blakemore, R. L. Milot, J. F. Hull, H. E. Song, L. Cai, C. A. Schmuttenmaer, R. H. Crabtree and G. W. Brudvig, *Energy Environ. Sci.*, 2011, **4**, 2389–2392; (*c*) P. K. Poddutoori, J. M. Thomsen, R. L. Milot, S. W. Sheehan, C. F. A. Negre, V. K. R. Garapati, C. A. Schmuttenmaer, V. S. Batista, G. W. Brudvig and A. Van Der Est, *J. Mater. Chem. A*, 2015, **3**, 3868–3879; (*d*) M. Yamamoto, Y. Nishizawa, P. Chábera, F. Li, T. Pascher, V. Sundström, L. Sun and H. Imahori, *Chem. Commun.*, 2016, **52**, 13702–13705.

5 O. Suryani, Y. Higashino, J. Y. Mulyana, M. Kaneko, T. Hoshi, K. Shigaki and Y. Kubo, *Chem. Commun.*, 2017, **53**, 6784–6787.

6 (*a*) F. Ronconi, Z. Syrgiannis, A. Bonasera, M. Prato, R. Argazzi, S. Caramori, V. Cristino and C. A. Bignozzi, *J. Am. Chem. Soc.*, 2015, **137**, 4630–4633; (*b*) J. T. Kirner and R. G. Finke, *ACS Appl. Mater. Interfaces*, 2017, **9**, 27625–27637; (*c*) J. T. Kirner, J. J. Stracke, B. A. Gregg and R. G. Finke, *ACS Appl. Mater. Interfaces*, 2014, **6**, 13367–13377; (*d*) M. Bonchio, Z. Syrgiannis, M. Burian, N. Marino, E. Pizzolato, K. Dirian, F. Rigodanza, G. A. Volpato, G. La Ganga, N. Demitri, S. Berardi, H. Amenitsch, D. M. Guldi, S. Caramori, C. A. Bignozzi, A. Sartorel and M. Prato, *Nat. Chem.*, 2019, **11**, 146–153.

7 (*a*) P. Bornoz, M. S. Prévot, X. Yu, N. Guijarro and K. Sivula, *J. Am. Chem. Soc.*, 2015, **137**, 15338–15341; (*b*) J. Chen, P. Wagner, L. Tong, G. G. Wallace, D. L. Officer and G. F. Swiegers, *Angew. Chem., Int. Ed.*, 2012, **51**, 1907–1910; (*c*) J. Chen, P. Wagner, L. Tong, D. Boskovic, W. Zhang, D. Officer, G. G. Wallace and G. F. Swiegers, *Chem. Sci.*, 2013, **4**, 2797.

8 (*a*) F. Li, K. Fan, B. Xu, Q. Daniel, L. Sun, L. Li and E. Gabrielsson, *J. Am. Chem. Soc.*, 2015, **137**, 9153–9159; (*b*) K. R. Wee, B. D. Sherman, M. K. Brennaman, M. V. Sheridan, A. Nayak, L. Alibabaei and T. J. Meyer, *J. Mater. Chem. A*, 2016, **4**, 2969–2975.

9 (*a*) A. Coletti, S. Lentini, V. Conte, B. Floris, O. Bortolini, F. Sforza, F. Grepioni and P. Galloni, *J. Org. Chem.*, 2012, **77**, 6873–6879; (*b*) M. Bonomo, F. Sabuzi, A. Di Carlo, V. Conte, D. Dini and P. Galloni, *New J. Chem.*, 2017, **41**, 2769–2779; (*c*) F. Sabuzi, S. Lentini, F. Sforza, S. Pezzola, S. Fratelli, O. Bortolini, B. Floris, V. Conte and P. Galloni, *J. Org. Chem.*, 2017, **82**, 10129–10138; (*d*) F. Sabuzi, V. Armuzza, V. Conte, B. Floris, M. Venanzi, P. Galloni and E. Gatto, *J. Mater. Chem. C*, 2016, **4**, 622–629.

10 (*a*) A. Sartorel, N. D. McDaniel, S. Bernhard and M. Bonchio, *J. Am. Chem. Soc.*, 2008, **130**, 5006–5007; (*b*) J. Fielden, J. M. Sumliner, N. Han, Y. V. Geletii, X. Xiang, D. G. Musaev, T. Lian and C. L. Hill, *Chem. Sci.*, 2015, **6**, 5531–5543; (*c*) M. Orlandi, R. Argazzi, A. Sartorel, M. Carraro, G. Scorrano, M. Bonchio and F. Scandola, *Chem. Commun.*, 2010, **46**, 3152–3154.

11 (*a*) B. H. Solis and S. Hammes-Schiffer, *Inorg. Chem.*, 2014, **53**, 6427–6443; (*b*) D. R. Weinberg, C. J. Gagliardi, J. F. Hull, C. F. Murphy, C. A. Kent, B. C. Westlake, A. Paul, D. H. Ess, D. G. McCafferty and T. J. Meyer, *Chem. Rev.*, 2012, **112**, 4016–4093; (*c*) S. Hammes-Schiffer, *J. Am. Chem. Soc.*, 2015, **137**, 8860–8871; (*d*) J. J. Warren and J. M. Mayer, *Biochemistry*, 2015, **54**, 1863–1878.

12 (*a*) F. Puntoriero, S. Serroni, G. La Ganga, A. Santoro, M. Galletta, F. Nastasi, E. La Mazza, A. M. Cancelliere and S. Campagna, *Eur. J. Inorg. Chem.*, 2018, 3887–3899; (*b*) M. Natali, F. Nastasi, F. Puntoriero and A. Sartorel, *Eur. J. Inorg. Chem.*, 2019, 2027–2039.

13 S. Berardi, V. Cristino, M. Canton, R. Boaretto, R. Argazzi, E. Benazzi, L. Ganzer, R. Borrego Varillas, G. Cerullo, Z. Syrgiannis, F. Rigodanza, M. Prato, C. A. Bignozzi and S. Caramori, *J. Phys. Chem. C*, 2017, **121**, 17737–17745.

14 (*a*) K. L. Materna, R. H. Crabtree and G. W. Brudvig, *Chem. Soc. Rev.*, 2017, **46**, 6099–6110; (*b*) R. Brimblecombe, A. Koo, G. C. Dismukes, G. F. Swiegers and L. Spiccia, *J. Am. Chem. Soc.*, 2010, **132**, 2892–2894.

15 B. D. Sherman, M. V. Sheridan, C. J. Dares and T. J. Meyer, *Anal. Chem.*, 2016, **88**, 7076–7082.

16 C. Besson, Z. Huang, Y. V. Geletii, S. Lense, K. I. Hardcastle, D. G. Musaev, T. Lian, A. Proust and C. L. Hill, *Chem. Commun.*, 2010, **46**, 2784–2786.